Investigation of sediment erosion phenomenon for different blade angle distribution in Francis runner

Abstract no: ID 60186

Investigation of sediment erosion phenomenon for different blade angle distribution in Francis runner

N Acharya[1*], C Trivedi[1], S Gautam[2] and O G Dahlhaug[1]
[1]Waterpower Laboratory, Department of Energy & Process Engineering, Norwegian University of Science and Technology, NO-7491, Trondheim, Norway
[2]Turbine Testing Lab, Department of Mechanical Engineering, Kathmandu University, Dhulikhel, Nepal
*Corresponding author (nirmal.acharya@ntnu.no)

Abstract. Wear and tear of hydraulic turbine due to sediment erosion is one of the major problems in hydropower plants located in the Himalayan and Andes regions. High sediment concentration in water of such areas wears down the mechanical components rapidly which causes significant operational challenges. In the present work, a prototype high head Francis runner with speed number 0.32 has been considered as reference case and other designs have been obtained modifying the blade angle distribution with same hydraulic parameters. Full turbine steady state numerical calculations were carried out at the best efficiency point and corresponding performance and erosion pattern are observed. Hydraulic efficiency and sediment erosion rate density are compared for the different cases taken into consideration. Sediment erosion analysis gives an indication of relative erosion intensity and critical zones of erosion damage in runner. Erosion was observed at the inlet near hub and shroud region and was mostly concentrated at the outlet of runner blades for all cases, where relative velocity is higher. Numerical results from CFD are also compared with the actual eroded turbine from the powerplant.

Keywords: CFD, Erosion rate density, Francis turbine, Runner blade, Sediment erosion

1. Introduction

Sediment particles along with water erodes the material surface of hydraulic turbine components in contact. Erosion effect in hydraulic turbine differs with the nature of flow inside the turbine. Francis runner cover the high head range of reaction turbines, which will get most serious damage from sand erosion due to availability of high velocities and high accelerations within [1]. Damage on the component depends on hardness of sediment, its shape and grain size along with the amount as well as the velocity. High relative velocity at the outlet and due to leakage flow carried out from clearance gaps of guide vanes (GVs), runner is exposed to the erosion phenomenon [2].

This paper examines the sediment erosion effect on runner at best efficiency point (BEP). Previous work focussed on the numerical analysis of guide vane of the same power plant [3]. Erosion pattern, erosion rate density and nature of vortices originating from leakage flow were observed during that study [3]. GV profiles with three different clearance gaps were compared and velocity on the vortex core was analyzed. To investigate the performance of Francis turbines and their erosion phenomenon, a MATLAB based code is applied to generate various blade profiles followed by CFD analysis on them.

2. Methodology

2.1 A brief description of the reference case and variation of blade angle distribution

Guide vanes and runner blades from prototype with speed number of 0.32 is considered as the reference case for this study, and the specifications are presented in Table 1.

Table 1. Design data for reference case

S.N.	Parameters	Value	Unit
1	Design head (H)	207	m
2	Discharge per unit (Q)	4.33	m^3/s
3	Rotational speed (N)	750	rpm
4	Power Output (P)	8	MW

Hydraulic design of the runner has a significant impact on the overall performance of the turbine [4]. The following study focusses to find the optimal runner design with a trade-off between performance and erosion behavior. This study focuses on comparison of sediment erosion investigation of 5 shapes of runner blades which were proposed for parametric study in previous works [5] [6] presented in Figure 1. Graph in fig. 1 shows relative length along the streamline in x- axis and distribution relative to inlet along y- axis which is enlarged for fig. 1(a) only whereas all other figures have similar parameters in x and y axis.

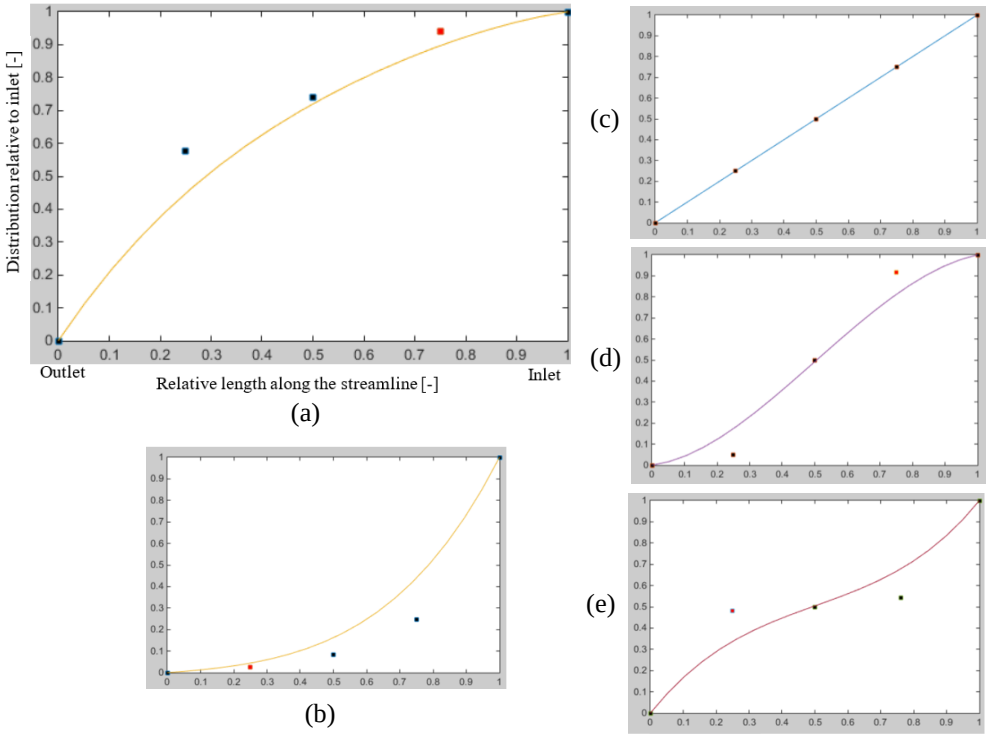

Figure 1 Blade angle distribution for various blades (a) Shape 1 (b) Shape 2 (c) Shape 3 (d) Shape 4 & (e) Shape 5

Velocities comprises of peripheral (U), absolute (C) and relative (W) at inlet and outlet of the runner as shown in fig. 2. Different shapes were obtained modifying the blade angle distribution from inlet to outlet. Blade angle is calculated from the equation 1 as follows:

$$tan\,\beta = \frac{C_m}{U - C_u} \quad [-] \tag{1}$$

where, C_m and C_u are meridional and tangential components of C respectively (Refer Fig. 2).

Design program has been made to generate blade profiles corresponding to blade angle distribution as input parameter. It controls how much hydraulic energy is converted to the mechanical energy in each section of blade. Adjusting the blade angle distribution influences blade loading which will affect the blade shape as well. In terms of energy conversion, shape 1 shows the blade angle distribution with low energy extraction at runner inlet and high energy extraction at the runner outlet as shown in fig. 1 (a), while shape 2 is opposite of it as shown in fig. 1 (b). A linear blade angle distribution is represented by shape 3 as in fig. 1 (c). Similarly, shape 4 & 5 shows the energy distributions with combinations of high and low energy distribution at the inlet and the outlet respectively which are depicted in fig. 1 (d) & 1 (e) [5].

Full model of the turbine consists of 13 runner blades and 16 GVs similar as in the power plant. Figure 3 shows isometric view of the reference runner.

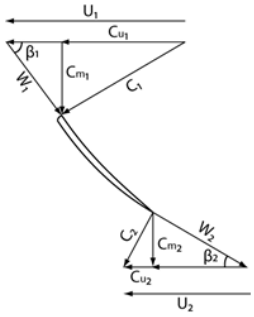

Figure 2 Velocity components on Francis runner blade

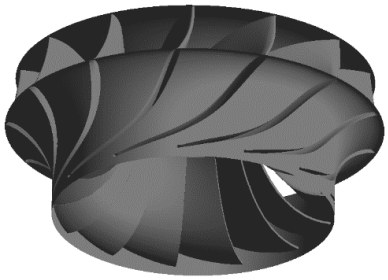

Figure 3 Isometric view of reference runner

2.2 Description of numerical and erosion model

Numerical calculation was done using ANSYS CFX by solving steady state RANS equations coupled with SST model for the turbulence quantities. Calculation was done using reduced geometry of the turbine that includes the guide vane cascade and runner blades. CFD simulations were carried out for reference runner blades with generated one together with same set of guide vanes ring. Numerical model of turbine was divided into 2 domains, GV (stationary) and a runner (rotating) at 750 rpm depicted in Figure 4. Mass flow rate of 4330 kg/s with prescribed velocity components in cylindrical co-ordinates at the inlet and static pressure outlet condition were chosen as boundary conditions. Non-slip wall condition is used for all wetted surfaces while frozen rotor interface is used for connecting non-conformal meshes with both stationary and rotating domains. High resolution advection scheme is used for all equations being solved. Designed mass flow rate of the turbine representing 100% flow was taken as BEP.

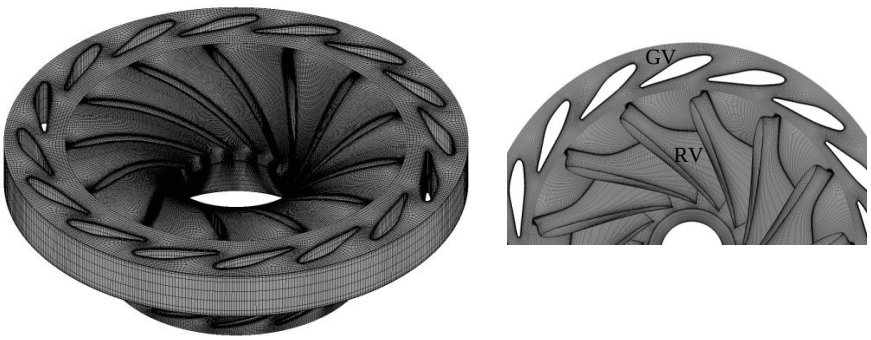

Figure 4 Domain with entire mesh size of 4.98 million elements

Sediment particle was defined as a spherical quartz material with a density of 2.65 gm/cm^3. Particle size distribution analysis of the collected sediment samples from the site showed the presence of particles with 150 µm diameter abundantly which can't be settled in desilting chamber and hence passes through the runner blades [7]. Particle mass flow rate was based on the maximum amount of sediment passing through the turbine unit that corresponds to 26028.7 tonnes /year recorded in the site in year 2013-2014 [8].

Tabakoff erosion model was chosen over Finnie for the simulations as it considers more parameters and is relatively more reliable and gives more realistic erosion rate indication [9]. It introduces the combination of higher and lower angle of attack of sediment particles in the surface. It considers the influence of quartz particles colliding with the ductile material which is somehow similar to the real scenario.

Tabakoff erosion model in ANSYS CFX, determines erosion rate *E* from the following relation:

$$E = f(\gamma)(V_p/V_1)^2 \cos^2\gamma\,[1 - R_T^2] + f(V_{PN}) \tag{2}$$

where, $f(\gamma) = [1 + k_2 k_{12} \sin(\gamma \frac{\pi/2}{\gamma_0})]^2$

$$R_T = 1 - V_p/V_3 \sin\gamma$$

$$f(V_{PN}) = (V_p/V_2 \sin\gamma)^4$$

$$k_2 = \begin{cases} 1.0 & if\ \gamma \le 2\gamma_0 \\ 0.0 & if\ \gamma > 2\gamma_0 \end{cases}$$

Here E is the dimensionless mass (mass of eroded wall material divided by the mass of particle). V_p is the particle impact velocity, γ is the impact angle in radians between the approaching particle track and the wall, γ_0 being the angle of maximum erosion. k_2 and k_{12} are model constants and depend on the particle/wall material combination.

Erosion of a wall due to a particle is computed from the following relation:

$$ErosionRate = E \times N \times m_p \tag{3}$$

Where, m_p is the mass of the particle and *N* is its number rate. The overall erosion of the wall is then the sum over all particles. This gives an erosion rate in [kg s^{-1}], and erosion rate density in [kg s^{-1} m^{-2}] to indicate the erosion area visually on the wall surface.

2.3 Mesh Sensitivity Analysis

Estimation of discretization error and extrapolation values was done by using the Grid Convergence Index (GCI) method [10]. It is considered as the effective method in predicting numerical uncertainties in the case of Francis turbines. Three types of structured hexahedral meshes with varying resolution were generated (coarse, medium and fine), initially starting from the coarsest grid that can achieve acceptable mesh quality and then increasing the element count throughout a structured refinement in all directions. Number of elements in each mesh equal to 1.67, 4.98 and 17.7 million. Turbine efficiency was chosen as monitored variable. These values obtained by the three mesh densities are noted as η_1, η_2 and η_3, where η_1 represents the results of the fine mesh and η_3 represents that of the coarse mesh. Overall grid refinement factor was then calculated with the ratio of the length of consecutive mesh scheme i.e. for $h_1 < h_2 < h_3$ and $r_{21} = h_2/h_1$, $r_{32} = h_3/h_2$. GCI value of the mesh was calculated as:

$$GCI_{fine}^{21} = \frac{1.25 e_a^{21}}{r_{21}^p - 1} \quad [-] \tag{4}$$

Where, e_a represents error in absolute value and r_{21} represents the grid refinement factor from medium mesh to fine mesh respectively. Results are summarized in Table 2. Considering the low discretization error that fine mesh has, it can be assumed that a fully grid independent solution has been achieved. However, as the medium mesh too gives balance results in terms of accuracy and computational time, the same has been used for all simulation cases.

Table 2. Discretization errors for B-III reference case

Efficiency as a variable measured for various sizes mesh		
No. of cells	N1, N2, N3 [10^6]	17.7, 4.98, 1.67
Grid refinement factor	r_{21}, r_{32}	1.52, 1.43
Efficiency	$\eta_1, \eta_2 \eta_3$	95.92, 96.83, 95.62
Apparent order	p	0.75
Extrapolated values	η_{ext}^{21}	94.18
Error estimates	e_a^{21}	0.95%
Extrapolated relative error	e_{ext}^{21}	1.84%
Fine grid convergence index	GCI $^{\eta}{}_{fine}$	2.26%
Medium grid convergence index	GCI $^{\eta}{}_{medium}$	3.6%

3. Results and discussions

3.1 Blade to blade plot for various shapes

Contour in the mid span of all blades is presented in Figure 5, which shows the velocity distribution from inlet to outlet for all blades.

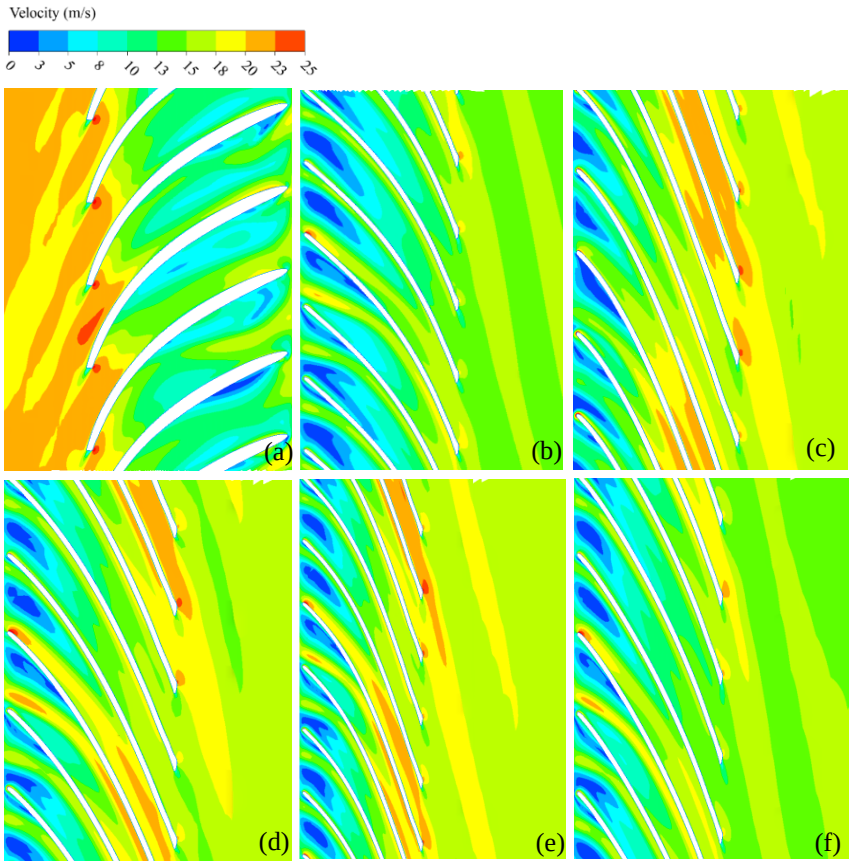

Figure 5 Velocity contours in runner at mid span (a) Reference (b) Shape 1 (c) Shape 2 (d) Shape 3 (e) Shape 4 & (f) Shape 5

Blade to blade transformation in turbo mode was acquired to observe the difference in blade profile for all shapes. Compared to reference blade profile, other blades are bit longer. Various velocity distributions were observed for different blade profile as depicted from Figure 5 (a) to 5 (f). It shows that the highest relative velocity is concentrated at the trailing edge in the reference blade clearly exhibited in fig. 5 (a) among all.

3.2 Comparison of sediment erosion for various shapes

Variation in pattern and amount of erosion in runner blade was observed with the effect of change of runner blade shapes. This study only focusses on the erosion of runner blades, so guide vanes erosion is excluded. As discussed in methodology section above, various shapes of the blades were obtained with the variation in blade angle distribution. Energy distribution is the distribution of product of peripheral velocity, U and peripheral component of absolute velocity, C_u. As U is only dependent on the radius and angular velocity, which is known for all points, C_u is strongly corelated to the blade angle distribution. Different blade angle distribution causes different transition from inlet to outlet velocity, which might explain the difference in erosion factors.

Figure 6 shows the normalized sediment erosion rate for different blades. Sediment erosion rate density for all blades is normalized with the erosion for reference case. From the bar graph, it is seen that reference blade shows the highest erosion factor of all followed by shape 3 which corresponds to the linear blade angle distribution. Shape 5 shows the lowest erosion rate of all which was followed by shape 1 and shape 2.

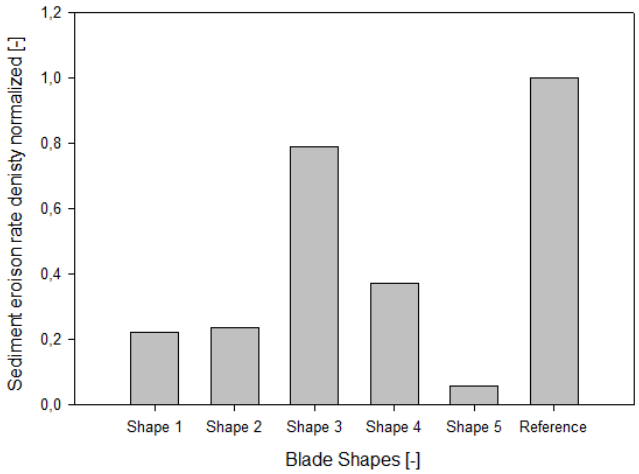

Figure 6 Erosion rate normalization for all blades

Figure 7 shows the plot of relative velocity versus streamwise location from inlet to outlet for all shapes. Values shows that the highest relative velocity is for the reference case followed by shape 3. Similarly, the smooth transition with the lowest relative velocity is acquired in case of shape 5. Shape 1 follows shape 5 closely with slight increase in velocity from middle section. Relative velocities for shape 2 and 4 fall in between maximum and minimum values. Figures 6 and 7 strongly exhibits the co-relation between relative velocity and erosion i.e. the higher possibility of erosion with the higher values of relative velocity at runner outlet.

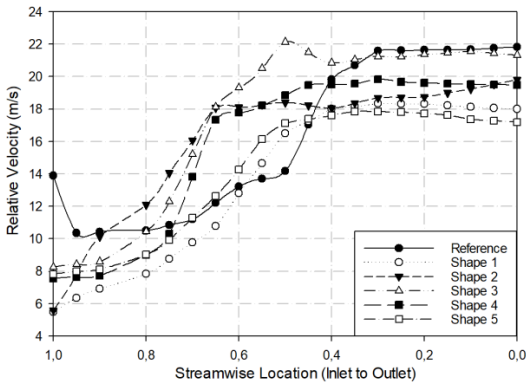

Figure 7 Comparison of relative velocity along blade span for all shapes

Numerical erosion model calculates the forces that acts when the particles (sediment in this case) collides with the wall where erosion rate indicates loss of material per square meter per second. Figure 8 shows the comparison of erosion at the inlet and outlet of the reference runner with CFD and field inspection. Erosion from CFD seen at the inlet and pattern of erosion near hub and shroud region was found to be similar as the inspected runner in the power plant as seen in figure 8 (a) & (b). Erosion was observed more adverse towards the outlet, where the relative velocity is higher. Erosion pattern obtained at the outlet is shown in figure 8 (c) which is quite similar with the eroded profile obtained from the site i.e. figure 8 (d). Erosion in the runner blades was mainly due to vortices travelling from clearance gaps that hits the inlet of runner and leaves the outlet with higher velocity. As the study was only done for best efficiency point (BEP) conditions, different erosion phenomena might occur for full load and part load conditions. At BEP, particle carried by flow regime is less turbulent and hence they glide with water rather than striking the blade surface and hence, minimum erosion is observed [11].

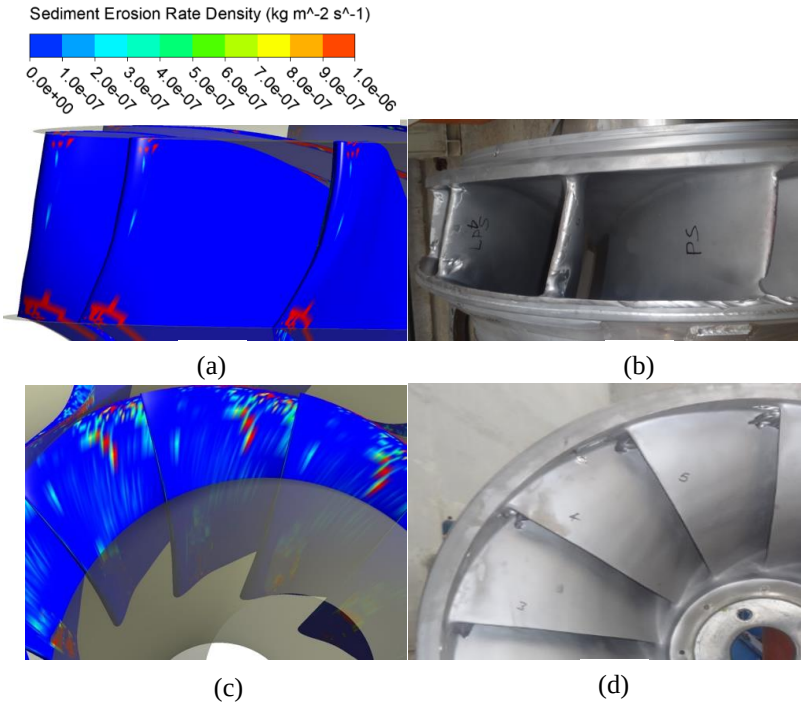

Figure 8 (a) Erosion at inlet of runner (b) Photograph of eroded profile at inlet (c) Erosion at outlet of runner and (d) Photograph of eroded profile at outlet

3.3 Comparison of efficiency for various shapes

Figure 9 shows the efficiency for five different types of runner blades generated. which is normalized upon reference blade. η* plotted on y-axis in figure 9 is the normalized efficiency based upon the reference blade.

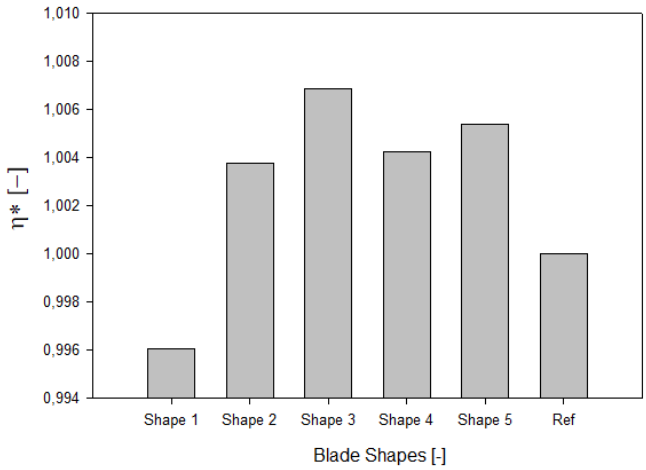

Figure 9 Normalized efficiency for various blades

In all cases, flow conditions are represented by GV opening angles corresponding to best efficiency point (BEP). Shape 3 shows the best efficiency followed by shape 5. Shape 2 and 4 shows somehow similar efficiency. Shape 1 shows the lowest efficiency among all blade designs.

4. Conclusion

Sediment erosion analysis gives an indication of relative erosion intensity and critical zones of erosion damage in turbine components. Numerical analysis on reference runner and 5 other different designs as per varying blade angle distribution was carried out. Erosion pattern, erosion rate density and efficiency were compared during the process.

It was seen that erosion pattern in runner blades predicted by CFD matches with erosion in actual turbine as seen in figure 8. Erosion was observed at the runner inlet near hub and shroud region and was mostly concentrated at the outlet of runner blades for all cases. Comparing the erosion rate for different blade profiles, shape 5 showed the optimum result whereas shape 3 showed the highest efficiency. Reference blade has highest relative velocity at outlet among all with rapid transition from section to section, which might be one of the major causes for highest erosion density rate. Shape 3 representing linear blade angle distribution, which has been commonly accepted for Francis runner design [5] stands out with highest efficiency but due the high relative velocity, it is also subjected to high sediment erosion. Varying blade angle distribution changes the blade profile which also seemed to yield a better reduction in erosion.

Optimization approach used for this study uses the same energy distribution from shroud to hub together with all streamlines for one shape. Better results can be obtained from different sort of energy distribution from hub to shroud in a single shape as well, which is yet to be investigated. Other operating conditions and sediment size & concentration should also be investigated. Several other distributions and combinations should be attempted to obtain the best trade-off between performance and erosion phenomenon during optimization process.

5. Further Works

Parametric design tool is being developed in MATLAB to carry out its hydraulic design and consequently optimization of the same. The main design philosophy is to minimize the velocity of water along the components such that sediment velocity will also be reduced. Erosion tendency function will be incorporated in the program and it can be used to develop several designs to look at measures for reducing erosion.

References

[1]. Brekke H, Wu Y.L. and Cai B.Y 2001 Design of hydraulic machinery working in sand laden water Abrasive erosion and corrosion of hydraulic machinery, volume 2, chapter 4, page 155-181 Imperial College Press
[2]. Thapa B.S, Thapa B and Dahlhaug O.G, Empirical modeling of sediment erosion in Francis turbines, *Energy* 4 (1) (2012) 386–391
[3]. Acharya N, Trivedi C, Wahl N. M, Gautam S, Chitrakar S and Dahlhaug O. G, Numerical study of sediment erosion in guide vanes of a high head Francis turbine 2019 Journal of Physics: Conference Series1266 012004
[4]. Iliev I, Trivedi C and Dahlhaug O.G 2018 Simplified hydrodynamic analysis on the general shape of the hill charts of Francis turbine using shroud- streamline modeling Journal of Physics: Conference Series1042 012003
[5]. Eltvik M 2013 *Sediment erosion in Francis turbines*, PhD Thesis, NTNU
[6]. Gjøsæter K, 2011, *Hydraulic Design of Francis Turbine Exposed to Sediment Erosion*, Master's Thesis, NTNU
[7]. Gautam S, Neopane H.P, Acharya N, Chitrakar S, Thapa B.S and Zhu B 2019 Sediment erosion in low specific speed francis turbines: A case study on effects and causes, *Wear*
[8]. Koirala R, Thapa B, Neopane H.P, Zhu B 2017 A review on flow and sediment erosion in guide vanes of Francis turbines, *Renewable and Sustainable Energy Reviews*
[9]. Eltvik M 2009 *Sediment erosion in Francis turbines*, Master Thesis, Norwegian University of Science and Technology
[10]. Celik I, Ghia U, Roache P, Freitas C, Coleman H and Raad P 2008 Procedure for estimation and reporting of uncertainty due to discretization in CFD applications, *Journal of Fluids Engineering, ASME,* 130(7), 078001
[11]. Shrestha K.P, Chitrakar S, Thapa B and Dahlhaug O.G 2018 Performance comparison of optimized designs of Francis turbines exposed to sediment erosion in various operating conditions, Journal of Physics: Conference Series1042 012001

Acknowledgment

This work was conducted under research project FME-Hydrocen. This project (No. 90148312) was funded by Norwegian Research Council and Norwegian Hydropower Industries.